Research Square

Preprints are preliminary reports that have not undergone peer review.
They should not be considered conclusive, used to inform clinical practice,
or referenced by the media as validated information.

Toward plasma-assisted fuel synthesis from CO_2 and water: Ethanol detection with Fe-loaded LTA zeolite

Shinfuku Nomura

nomura.shinfuku.mg@ehime-u.ac.jp

Ehime University

Ayano Imai

Oono Associates

Tomoya Ishii

Ehime University

Ryota Shiba

Oono Associates

Junichi Nakajima

Ehime University

Research Article

Keywords: in-liquid plasma, Fe-loaded LTA zeolite, ethanol, oxygenates, carbon dioxide

Posted Date: November 25th, 2026

DOI: https://doi.org/10.21203/rs.3.rs-11672289/v1

License: This work is licensed under a Creative Commons Attribution 4.0 International License.
Read Full License

Additional Declarations: Competing interest reported. Ayano Imai and Ryota Shiba are employees of Oono Development Co., Ltd., which provided research support for this study.

Toward plasma-assisted fuel synthesis from CO_2 and water: Ethanol detection with Fe-loaded LTA zeolite

Shinfuku Nomura[1]*, Ayano Imai[2], Tomoya Ishii[1], Ryota Shiba[1,2] Junichi Nakajima[1]

* Corresponding author:
Shinfuku Nomura
E-mail address: nomura.shinfuku.mg@ehime-u.ac.jp

[1] Graduate School of Science and Engineering, Ehime University, Matsuyama 790-8577, Japan
[2] Institute of Environmental Sciences and Technology, Oono Associates, Tōon-shi, Ehime 791-0321, Japan

Abstract

Fe-loaded Linde type A (LTA) zeolite was examined in a material screening study of in-liquid plasma treatment of CO_2-supplied water. Among the materials screened, Fe/LTA gave the highest quantified ethanol amount. At a nominal Fe amount of 10 mmol, treatment at 4 kV and 50 kHz for 15 min with a CO_2 flow rate of 2.0 L min^{-1} yielded recovered amounts of 68.33 μg ethanol and 2.43 μg acetone. Estimated limits of quantification of 0.372, 0.342 and 0.112 mg L^{-1} for acetone, methanol and ethanol, respectively, were applied to individual liquid fractions; methanol was at or below its estimated limit. Ethanol accounted for 95.9% of the uncorrected quantified carbon subtotal for these three compounds. Selected-ion monitoring chromatograms showed a response near the ethanol-standard retention time for Fe/LTA under CO_2 with plasma. This response was more prominent than those in the displayed plasma-off, Ar-plasma, bare-LTA and pure-water control traces. These findings identify Fe/LTA as a material of interest for aqueous plasma processing toward fuel synthesis from CO_2 and water.

Keywords: in-liquid plasma; Fe-loaded LTA zeolite; ethanol; oxygenates; carbon dioxide

1 Introduction

Synthetic fuels produced from recycled CO_2 and hydrogen are being investigated to support carbon neutrality, improve resource security and store renewable energy in chemical form [1]. Established routes include Fischer–Tropsch synthesis, which converts CO/H_2 syngas into liquid hydrocarbons, and the Sabatier reaction, which converts CO_2 and H_2 into methane. In CO_2-based Fischer–Tropsch pathways, CO_2 must first be converted into a suitable carbon-containing feed, commonly through reverse water–gas shift or co-electrolysis. Both fuel-synthesis routes require hydrogen, making its production, supply and associated energy demand central process considerations. Recycling carbon into fuels can reduce reliance on fossil carbon, but its climate benefit depends on the carbon source and the energy used throughout the process [1].

Direct conversion of CO_2 and water into alcohols would enable water to serve as the hydrogen-bearing feedstock without a separate H_2 supply during conversion. This goal is central to artificial photosynthesis, and plasma conversion of CO_2/H_2O has been discussed in that context [2]. Artificial photosynthesis conventionally uses light-driven chemistry [3]; plasma provides an electrically driven approach toward the same fuel-forming objective. Coupling plasma with renewable electricity could therefore support carbon recycling and chemical energy storage. The present study explores the choice of solid material for an aqueous plasma process directed toward this objective.

Plasma processing offers an electrically driven route to CO_2 activation [4,5]. Combining plasma with solids can alter discharge behavior and surface chemistry, making the choice of material and the plasma–surface interaction important design variables [2,6–10]. Synergistic activation has also been reported for dielectric-barrier discharge plasma combined with a photocatalyst [11]. In aqueous systems, interfacial transport and subsequent liquid-phase reactions further influence the products recovered [12]. These multiple contributions make it necessary to distinguish recovered product amounts from intrinsic catalytic activity.

Early microwave-plasma studies of CO_2/H_2O reported oxalic acid and H_2O_2 [13,14] and, subsequently, methanol, including during plasma removal of deposited material [15]. Surface-wave microwave discharges produced syngas from CO_2 and water vapor [16], while a dielectric-barrier-discharge study identified competing recombination reactions [17]. Catalytic systems including NiO/TiO_2 [18], Ni/Al_2O_3 [19], NiO/cordierite [20] and Ni- or Cu-based materials [21] have also been examined. These gas-phase studies provide context for aqueous Fe/LTA screening [22].

At plasma–liquid interfaces, solvated electrons have been measured [23], and organic acids or their conjugate anions have been reported during plasma treatment of CO_2-containing water [24–26]. Related aqueous peroxide chemistry further illustrates the range of reactions in plasma–liquid systems [27]. Our group previously investigated plasma generation in hydrocarbon liquids [28], discharge characteristics in water [29] and plasma-containing bubble growth [30], followed by oxygenate formation from aqueous sodium carbonate [31] and ethanol detection using CO_2 and water as feedstocks [32].

Our earlier study of methanol decomposition motivated the introduction of catalytic materials into the present system [33]. Incorporating catalytic metal through an electrode and plate configuration increased the hydrogen production rate by up to 3.5-fold, with the highest performance obtained using a Ni electrode and plate. This result showed that integrating catalytic metal with an in-liquid discharge can enhance chemical conversion. It prompted the present investigation of whether metal-containing solids influence the oxygenates recovered from CO_2-supplied water. Fe-loaded LTA was included in this exploratory screening to examine the hypothesis under the different feed conditions used here.

Related CO_2/H_2 plasma-catalytic studies have examined methanol synthesis with discharge-activated catalysts [34], $Cu/\gamma\text{-}Al_2O_3$ [35] and Ni–Co interfaces [36]. Oxygenates have also been produced from CO_2/CH_4 [37,38], while water addition promoted ethanol production over Cu_2O/CeO_2 during CO_2 hydrogenation [39]. Operando studies of Cu–Zn/ZSM-5 identified metallic Cu and Cu/ZnO interfaces involved in methanol synthesis [40]. The additional H_2 or CH_4 feeds and different discharge configurations limit direct performance comparisons with the present aqueous screening [41].

Adsorption measurements on zeolites and silica [42], plasma-assisted reforming with zeolite 5A [43] and $SiO_2@TiO_2$ packing studies [44] also motivate examining the roles of the support and metal separately. Here, we screen Fe/LTA alongside Fe/SiO_2, Zn-containing materials, Cu/LTA and ZSM-5 to identify materials of interest for aqueous plasma processing. Selected-ion monitoring (SIM) chromatograms in the ethanol retention region are compared with bare-LTA, plasma-off, Ar-plasma and pure-water controls. This combination of material screening and qualitative controls provides the basis for evaluating the Fe/LTA observation and its relevance to direct CO_2/H_2O fuel synthesis.

2 Materials and methods

2.1 Preparation of the solid materials

Zeolite-supported materials were prepared using 40 g of support and 3 L of an aqueous metal-salt solution containing 0.1 mol L^{-1} metal. The support was suspended in 1 L of solution, stirred for 30 min and allowed to stand for 10 min. After centrifugation at 3000 × g for 10 min, the supernatant was replaced with fresh solution. Three contact cycles were performed, with a final 24 h aging period in the third suspension. No washing step was performed. After removal of the supernatant, the remaining solid-containing fraction was frozen in liquid nitrogen and freeze-dried overnight. The dried material was calcined in air at 500 °C for 1 h with a heating rate of 20 °C min^{-1}, then treated at 500 °C for 1 h under H_2 and Ar supplied at 200 and 1000 mL min^{-1}, respectively. The material was cooled to room temperature under Ar. The heating rate during reduction was not specified.

Silica-supported materials were prepared using 40 g of silica, a metal precursor corresponding to a nominal metal loading of 5 wt%, and 100 mL of pure water. The sealed suspension was aged at room temperature for 24 h and subjected to the same drying, calcination and reduction sequence. Metal uptake was assumed to occur predominantly through surface adsorption rather than ion exchange; this assignment was not independently established. After preparation, the materials were collected in sealed Ar-filled containers and used in plasma experiments within 1 h of collection. Metal contents were estimated by scanning electron microscopy coupled with energy-dispersive X-ray spectroscopy (SEM–EDS). Table 1 summarizes these estimates, specimen masses and calculated metal amounts. The mass of reduced material used in each experiment was calculated from the measured metal mass

Table 1. Metal contents estimated by SEM–EDS, specimen masses and calculated metal amounts. The metal contents are semi-quantitative area averages (wt%). Metal amounts were calculated from these mass fractions and specimen masses; they do not specify active-site populations.

Material	Metal EDS wt%	Specimen g	Metal amount mmol, calculated
Untreated LTA	—	0.68	—
Fe/LTA	44.35	1.25	9.93
Fe/SiO_2	5.84	4.78	4.99
Zn/LTA	16.65	19.64	50.0
Zn/SiO_2	4.40	1.42	0.96
Cu/LTA	28.0	2.27	10.0

fraction and metal molar mass to obtain the prescribed nominal metal amount. The nominal metal amounts identify the experimental conditions and do not specify the number or oxidation state of active sites.

2.2 Plasma treatment and product analysis

Figure 1 shows a conceptual diagram of the in-liquid plasma apparatus. The apparatus comprised a quartz-glass reactor, hollow Cu–W electrodes, a pulse power supply (MPP04-A4-200-A, Kurita Seisakusho), a quartz rod, a condenser and an optical emission spectrometer. The reactor had upper and lower rubber stoppers and lateral electrode ports, an internal diameter of 35.5 mm and a reported maximum capacity of 70 mL. Each experiment used 50 mL of pure water. The semicircular hollow electrodes had a nominal Cu:W composition ratio of 20:80, outer and inner diameters of 3 and 1 mm, respectively, and an interelectrode gap of 1 mm. Treatment was conducted at atmospheric pressure under laboratory conditions, with operating settings of 4 kV and 50 kHz, a CO_2 flow rate of 2.0 L min^{-1} and a discharge duration of 15 min. The reactor liquid was allowed to cool naturally during batch operation. Volatile components were collected using a condenser set to 2 °C; this setpoint does not specify the reactor-liquid temperature. Average absorbed power was not measured.

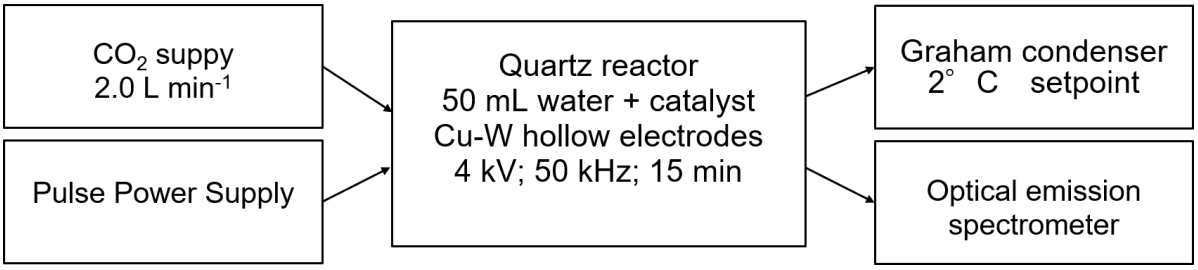

Fig. 1. Conceptual diagram of the in-liquid plasma apparatus. Connections indicate component functions rather than exact plumbing, geometry or sampling locations. The condenser setpoint is distinct from the reactor-liquid temperature.

Acetone, methanol and ethanol were analyzed by gas chromatography–mass spectrometry (GC–MS; GCMS-QP2010 Ultra, Shimadzu) using a DB-WAX column. The column and injector temperatures were 65 and 200 °C, respectively, and the injection volume was 5 μL. Undiluted samples were quantified using external-standard calibration curves. Each collected sample was analyzed once, and recovery was not evaluated. Selected-ion monitoring (SIM) chromatograms at m/z 31, 45 and 46 were used to compare an ethanol standard (5 mg L^{-1}), Fe/LTA under CO_2 with plasma, and plasma-off, Ar-plasma, bare-LTA and pure-water controls.

These chromatograms were used for qualitative comparison, rather than for additional product-mass calculations, and were not treated as independent quantitative replicates.

Estimated LOQs were calculated by response scaling as $C_{est} = C_{ref} \times R_{threshold} / R_{ref}$, where C_{ref} = 5 mg/ L and R_{ref} and $R_{threshold}$ are the reference and threshold responses in the analytical calculation record. The response pairs (R_{ref}, $R_{threshold}$) were (19479, 1450), (10747, 735) and (41010, 915) for acetone, methanol and ethanol, respectively, giving estimated LOQs of 0.372, 0.342 and 0.112 mg L^{-1}. This calculation assumes a proportional response with a negligible intercept. These estimates were applied as common reporting thresholds to all samples. Concentrations at or below the corresponding unrounded estimate were excluded from numerical sums. These response-based estimates are reporting thresholds rather than validated method quantification limits [45]. Accuracy and precision near the thresholds were not independently established, and further method validation is required [46].

Condensate fractions were collected at nominal times of 5, 10 and 15 min; residual reactor liquid was collected after the 15 min treatment. Condensate was collected in successive 5 min intervals when sufficient volume was available. If the volume at 5 min was insufficient for analysis, collection continued to 10 min and a cumulative fraction was collected. Liquid volumes were measured using syringes or graduated cylinders. The quantified amount of each compound in a fraction was calculated as concentration (μg mL^{-1}) multiplied by collected volume (mL). Reported amounts are the sums of quantified contributions from condensate fractions and residual reactor liquid. Contributions at or below the estimated LOQ were not assigned numerical masses.

Calculations used unrounded values. The Fe/LTA ethanol amount comprised 65.9054 μg in the reactor liquid and 2.42649 μg in the fraction designated “15 min”. Ethanol in the fractions designated “5 min” and “10 min” was at or below the estimated LOQ. These fractions are not independent experimental replicates. The two Cu/LTA records were reported separately, without pooling them or treating them as a validated replicate series.

Liquid chromatography (LC) and ion chromatography (IC) provided complementary, provisional peak assignments for Fe/SiO_2 at a nominal Fe amount of 5 mmol. Optical emission spectroscopy was used to examine emitting species in the plasma. Plasma diagnostics can help characterize reactive species [47], but validation is specific to the diagnostic method and plasma–liquid system [48]. Screening results are presented descriptively, without significance tests or error bars, because independent experimental replication and analytical uncertainties have not been established.

2.3 Data treatment

For each quantified compound, its carbon amount was calculated as

$$n_C = m \times N_C / M \qquad (1)$$

where m is the retained quantified mass (μg), N_C is the number of carbon atoms per molecule and M is the molar mass (g / mol); n_C is expressed in μmol C. Molar masses of 58.08, 32.04 and 46.07 g /mol were used for acetone, methanol and ethanol, respectively. Values at or below the estimated LOQ are denoted by ≤ LOQ, which indicates neither a true zero nor a confirmed non-detection. No zero or fractional-LOQ substitution was used. Thresholds were applied to individual concentrations before multiplication by collected volumes. Carbon subtotals include only retained quantified contributions from these three compounds, so the sums need not represent complete recovered amounts. A compound's fraction of this subtotal describes the quantified product composition, rather than overall carbon selectivity. Comparisons use unrounded amounts, and no ratio is calculated when a required value is at or below the estimated LOQ. These amounts do not represent reaction rates, conversion or energy efficiency.

3 Results and discussion

3.1 Product distribution in the screening experiments

Table 2 summarizes the quantified product amounts and corresponding carbon subtotals for the screening experiments. Figure 2a compares the quantified product amounts, and Figure 2b compares their carbon subtotals. Fe/LTA gave the highest quantified ethanol amount among the listed screening records. After applying the common estimated LOQs, the quantified amounts were 68.33 μg ethanol and 2.43 μg acetone; methanol was at or below its estimated LOQ. Ethanol corresponded to 2.966 μmol C within a carbon subtotal of 3.092 μmol C, accounting for 95.9% of that subtotal. This percentage excludes unquantified fractions and unmeasured products and does not establish carbon selectivity from CO_2. These values were not blank-corrected; possible acetone contamination must be resolved before acetone and its contribution to the carbon subtotal can be attributed to the discharge.

Fe/SiO_2 at 5 mmol Fe gave 30.67 μg acetone and 0.21 μg methanol, with ethanol at or below its estimated LOQ. ZSM-5 gave 3.50 μg acetone. Zn/SiO_2 at 1 mmol Zn gave 0.18 μg methanol and 0.16 μg ethanol, whereas Zn/LTA at 50 mmol Zn gave 0.55 μg methanol and 0.21 μg ethanol; acetone was at or below its estimated LOQ in both cases. Cu/LTA records 1 and 2 at 10 mmol Cu gave 0.23 and 0.41 μg ethanol, respectively. Methanol was at or below its estimated LOQ in record 1 and amounted to 1.08 μg in record 2; acetone was at or below

its estimated LOQ in both records. Unequal metal amounts and the absence of established replication limit direct performance comparisons.

Table 2. Sums of retained quantified amounts and corresponding carbon subtotals. Estimated LOQs of 0.372, 0.342 and 0.112 mg L^{-1} for acetone, methanol and ethanol, respectively, were applied to individual fractions. ≤LOQ indicates at or below the estimated LOQ; these contributions were excluded without zero substitution. ZSM-5 is the recorded material label, and the dash indicates an unspecified metal amount. Cu/LTA records are listed separately. Uncertainty estimates were unavailable. Values have not been blank-corrected. Possible acetone contamination affects interpretation of the acetone amounts and carbon subtotals.

Material	Metal mmol	Acetone µg	Methanol µg	Ethanol µg	Subtotal µmol C
ZSM-5	—	3.50	≤ LOQ	≤ LOQ	0.181
Fe / SiO_2	5	30.67	0.21	≤ LOQ	1.591
Fe / LTA	10	2.43	≤ LOQ	68.33	3.092
Zn / SiO_2	1	≤ LOQ	0.18	0.16	0.012
Zn / LTA	50	≤ LOQ	0.55	0.21	0.026
Cu / LTA record 1	10	≤ LOQ	≤LOQ	0.23	0.010
Cu / LTA record 2	10	≤ LOQ	1.08	0.41	0.051

(a) Retained quantified product amounts

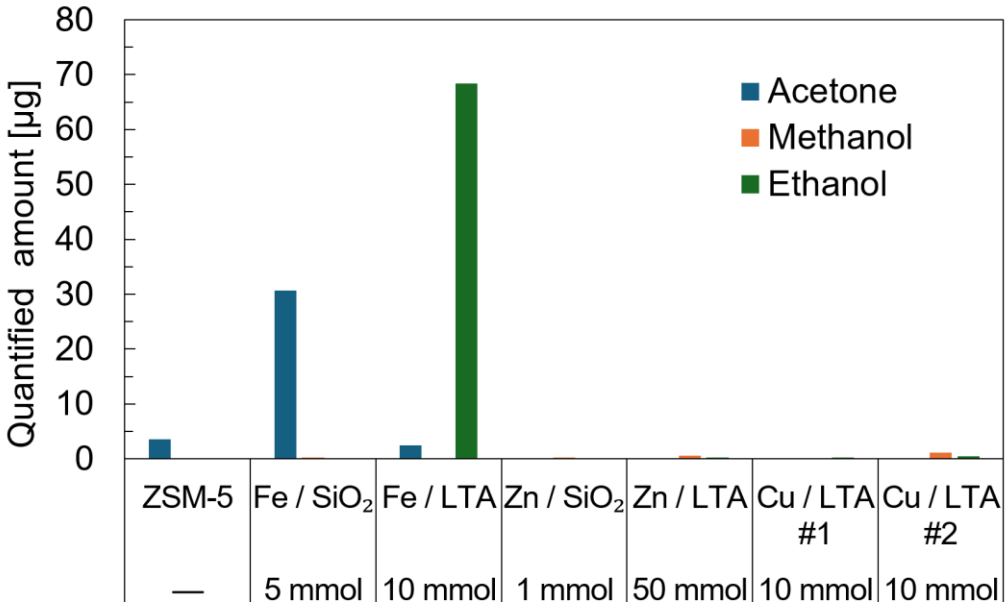

(b) Carbon subtotal of retained quantified compounds

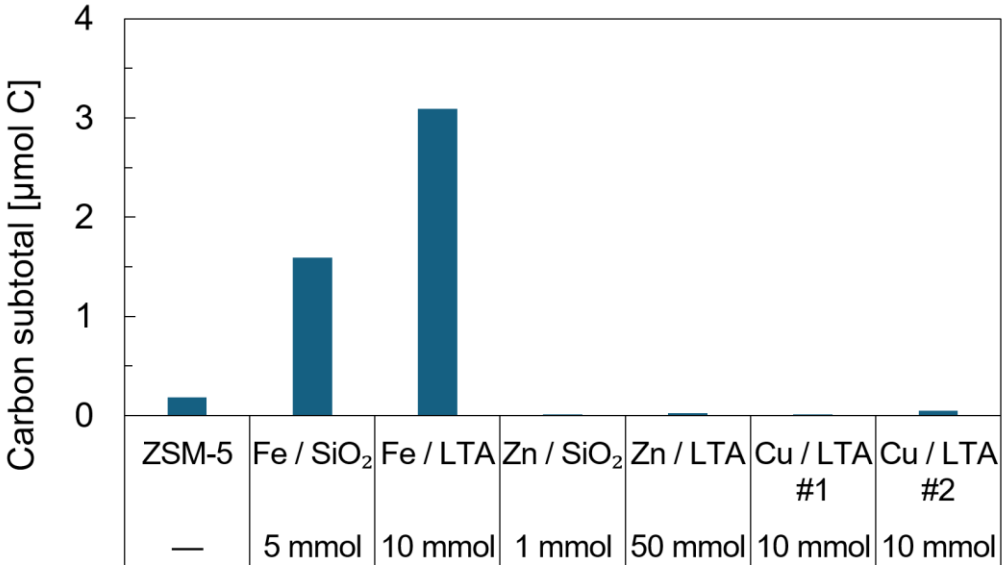

Fig. 2. Product distributions after applying common estimated LOQs to individual fractions: (a) retained quantified amounts and (b) corresponding carbon subtotals. Values marked ≤LOQ are unplotted and excluded without zero substitution. Cu/LTA records are shown separately. Metal amounts differ across conditions. Error bars are omitted because replication and uncertainties have not been established. Values have not been blank-corrected, and the acetone background remains unresolved.

3.2 Interpretation of material comparisons

Ethanol was at or below the estimated LOQ for Fe/SiO_2 at 5 mmol Fe and for ZSM-5. Consequently, neither condition provides a quantified denominator for calculating an ethanol enhancement factor relative to Fe/LTA. Fe/SiO_2 gave a larger quantified acetone amount than ZSM-5, but possible acetone contamination prevents attributing this difference to a material

effect. ZSM-5 is a comparison zeolite rather than a matched bare-LTA or bare-silica control. Comparisons across Fe/LTA, Zn-containing materials and Cu/LTA are also limited by differences in metal amount and material composition. The data do not establish reaction-rate enhancement or intrinsic catalytic activity.

3.3 Complementary analytical observations

Figure 3a shows the broad optical emission spectrum for Fe/LTA, with features provisionally assigned to H and O. Figure 3b shows the 300–320 nm region containing features provisionally assigned to OH, while Figure 3c shows the 420–440 nm region containing a feature provisionally assigned to CH. Cu emission was also indicated in the broad spectrum, consistent with possible electrode involvement. The absence of a distinct Fe emission signal does not exclude Fe-containing species, leaching or surface reactions. These spectra characterize the emitting species in the discharge but do not identify the carbon source of the recovered organics.

Figure 4 compares SIM chromatograms for the ethanol standard, Fe/LTA under CO_2 with plasma, and four control conditions. The Fe/LTA sample shows a response at approximately 1.82 min, near the main ethanol-standard retention region. No comparably prominent peak is apparent in the displayed plasma-off, Ar-plasma, bare-LTA or pure-water traces. These comparisons support further examination of the Fe/LTA–CO_2–plasma combination. However,weak responses may be obscured by the vertical scale, and the traces do not establish non-detection or concentrations below the estimated LOQ. Control concentrations and product masses were not validated; the 68.33 μg ethanol amount is the original, uncorrected screening result. Acetone-related responses were also reported in blank/control records. GC–MS waste handling was suggested as a possible contamination source, but this explanation remains unconfirmed.

For Fe/SiO_2 at 5 mmol Fe, LC peaks were provisionally assigned to formaldehyde at 8.374 min and acetaldehyde at 10.840 min; peaks at 12.120 and 14.293 min remained unidentified. IC peaks were provisionally assigned to acetate, formate and oxalate at 3.81, 4.33 and 15.59 min, respectively. These observations cannot be transferred to Fe/LTA, and retention times alone do not confirm a reaction sequence. IC results were excluded from quantitative comparisons because the concentration-to-mass conversion and ion-versus-acid reporting basis remain unresolved. Possible chloride-related matrix effects also require evaluation.

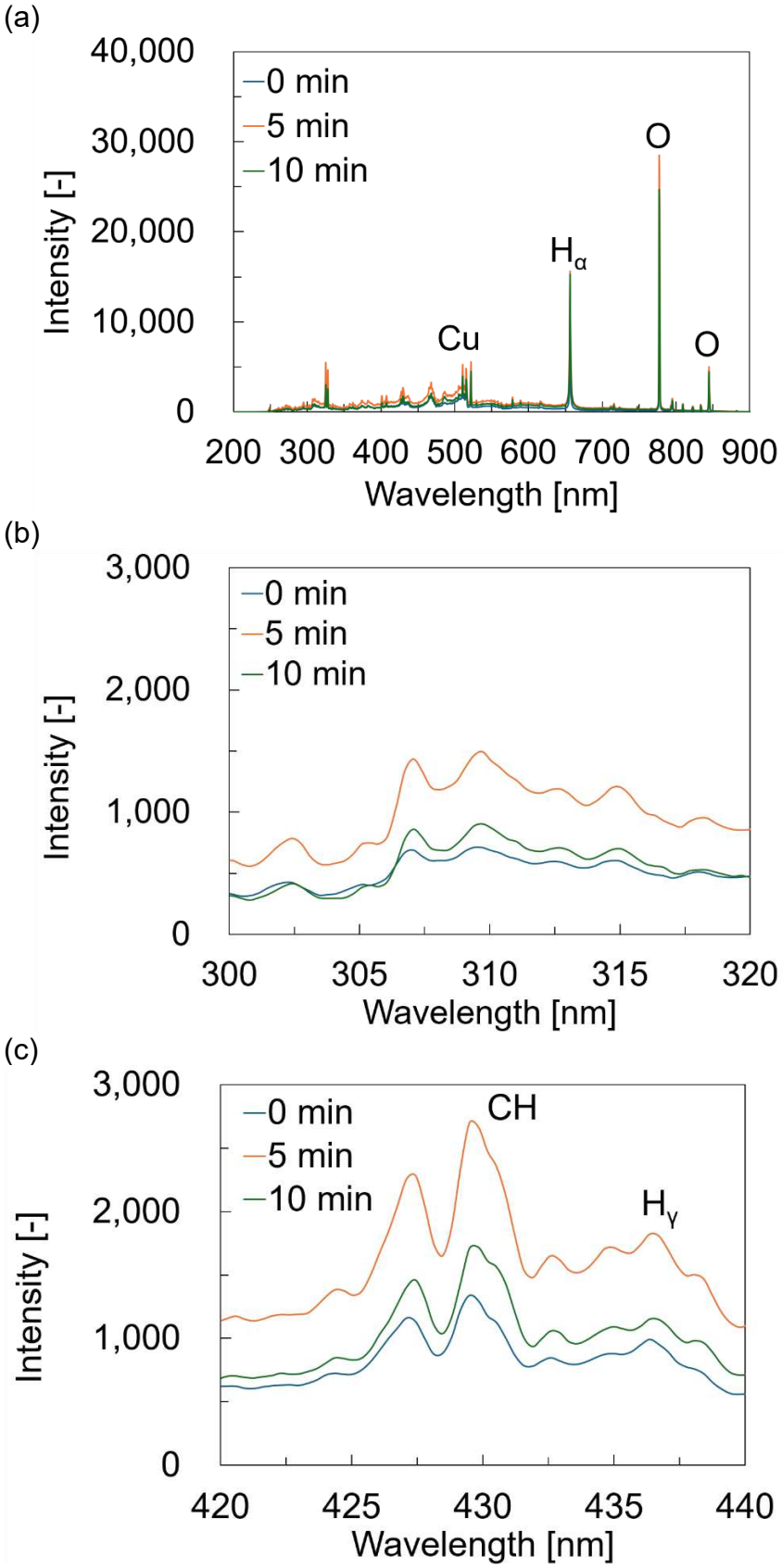

Fig. 3. Optical emission spectra for Fe/LTA: (a) broad spectrum, (b) 300–320 nm and (c) 420–440 nm. Spectra recorded at 0, 5 and 10 min are shown. Species assignments are provisional, including OH in (b) and CH in (c). Intensities are shown on the original scales and are not used to quantify radical concentrations or temperature.

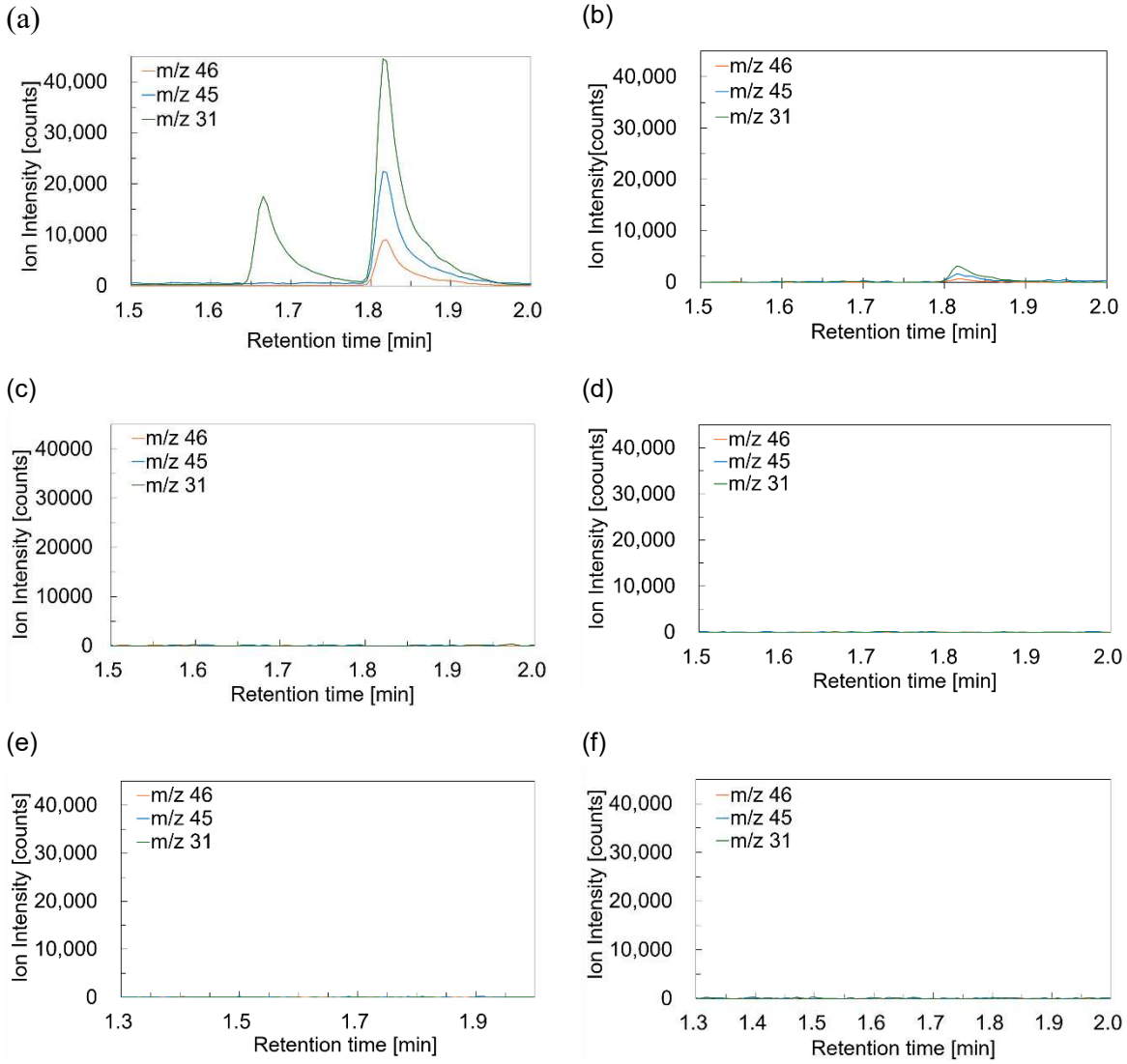

Fig. 4. SIM chromatograms at m/z 31, 45 and 46 for (a) an ethanol standard (5 mg/ L), (b) Fe/LTA under CO_2 with plasma, (c) Fe/LTA under CO_2 without plasma, (d) Fe/LTA under Ar with plasma, (e) bare LTA under CO_2 with plasma and (f) a pure-water blank. The traces are green for m/z 31, blue for m/z 45 and orange for m/z 46. Signals were baseline-shifted for visual comparison. The displayed traces support qualitative comparisons; control concentrations and non-detection were not established.

3.4 Interpretation and limitations

The ethanol-rich quantified product composition extends our earlier observations in aqueous sodium carbonate [31] and CO_2-supplied water [32] to Fe/LTA screening. Differences in feed chemistry and operating conditions prevent attributing cross-study differences to Fe addition. Water-assisted ethanol formation over Cu_2O/CeO_2 [39] and operando identification of Cu-related sites in Cu–Zn/ZSM-5 [40] motivate investigating water participation and metal speciation. These studies do not establish the same intermediates or C–C coupling pathway in

aqueous Fe/LTA. The oxalate-forming aqueous processes [25,26] also illustrate that different discharge environments can yield different liquid-product distributions.

Material addition can influence adsorption, product retention, discharge behavior and recovery as well as surface chemistry [8,12]. Gas-phase adsorption and plasma-packing studies [42–44] provide useful context, but do not quantify these contributions in liquid water. The catalytic enhancement in our methanol-decomposition study [33] motivates examining these effects in the present system. The qualitative controls provide an initial comparison; separating the contributions will require matched quantitative measurements and characterization of Fe loading, oxidation state and leaching.

Plasma-assisted CO_2 reduction to nanocarbon has been reported in water using dispersed gallium [49], illustrating a different material–product combination. Such findings do not establish the origin of the carbon in the present oxygenates. Quantified feed-gas controls and $^{13}CO_2$ tracing with isotopologue analysis would help resolve that origin. Earlier methanol detection during plasma removal of deposited material [15] underscores the need to examine retained carbon. Carbon-containing impurities, cleaning residues and material-derived contributions remain possible until excluded experimentally. The complexity of plasma interactions with organic-containing liquids also calls for system-specific interpretation [50]. The ethanol standard and blank/control traces provide useful qualitative comparisons, but product identification and low-concentration quantification still require validation of retention times, diagnostic ion ratios, blanks, calibration, precision and recovery [45,46].

The present measurements characterize recovered product amounts. Determining an apparent activation energy would require temperature-dependent kinetic measurements [51], while assessing CO_2 conversion, carbon yield and energy efficiency would require a complete carbon balance and absorbed-energy measurements [52]. These quantities were therefore outside the scope of the present screening.

4 Conclusions

Fe/LTA gave the highest quantified ethanol amount among the materials examined during in-liquid plasma treatment of CO_2-supplied water. At a nominal Fe amount of 10 mmol, treatment at 4 kV and 50 kHz for 15 min gave recovered amounts of 68.33 μg ethanol and 2.43 μg acetone, while methanol was at or below its estimated LOQ. Ethanol represented 95.9% of the quantified carbon subtotal for these three compounds. This uncorrected composition describes

the recovered products, rather than CO_2 selectivity; possible acetone contamination remains unresolved.

The response near the ethanol-standard retention time was more prominent in the displayed Fe/LTA–CO_2–plasma trace than in the plasma-off, Ar-plasma, bare-LTA and pure-water traces. Together with the material screening, this qualitative comparison identifies Fe/LTA as a material of interest for aqueous plasma processing. Optical emission measurements provide complementary observations of the discharge environment. The current measurements do not establish a quantitative catalytic enhancement, product carbon source or reaction pathway.

Motivated by the catalytic enhancement previously observed in methanol decomposition, this study extends our investigation of metal-containing materials in liquid-phase plasma reactions. It provides an experimental starting point for exploring CO_2 and water as feedstocks toward the fuel-forming objective of artificial photosynthesis, without a separate H_2 feed during plasma treatment. Independent replication, validated quantitative controls, carbon-source tracing and absorbed-power measurements would allow the Fe/LTA observation to be evaluated in terms of catalytic effects and the prospects for renewable-electricity-driven carbon recycling.

CRediT authorship contribution statement

S. Nomura: Conceptualization, Supervision, Writing – review and editing. A. Imai: Data curation, Writing – review and editing. T. Ishii: Methodology, Investigation, Formal analysis. R. Shiba: Methodology, Validation. J. Nakajima: Conceptualization, Writing – original draft. All authors have read and approved the manuscript.

Declaration of generative AI and AI-assisted technologies in the writing process

During manuscript preparation, OpenAI Codex was used to assist with revision, language editing, figure layout, and the identification and preliminary checking of references. AI-generated content was not treated as research evidence or as independent verification of published findings. The authors reviewed and edited the content and take full responsibility for the accuracy, integrity and originality of the manuscript, including its references, interpretations and figures.

Competing interests

Ayano Imai and Ryota Shiba are employees of Oono Development Co., Ltd., which provided research support for this study.

Funding

This work was supported by JSPS KAKENHI Grant Number 23K26051 and by Oono Development Co., Ltd.

Data availability

Access to project data is restricted by contractual confidentiality obligations and the need to protect undisclosed technical information. Measurement data, chromatograms and calibration curves may be made available upon request to the corresponding author, subject to these restrictions.

References

1. C. Graves, S.D. Ebbesen, M. Mogensen, K.S. Lackner, Sustainable hydrocarbon fuels by recycling CO_2 and H_2O with renewable or nuclear energy, Renewable and Sustainable Energy Reviews 15 (2011) 1−23. https://doi.org/10.1016/j.rser.2010.07.014.
2. R. Snoeckx, A. Bogaerts, Plasma technology − a novel solution for CO_2 conversion?, Chemical Society Reviews 46 (2017) 5805−5863. https://doi.org/10.1039/C6CS00066E.
3. International Union of Pure and Applied Chemistry, Artificial photosynthesis, in: Compendium of Chemical Terminology, 5th ed., 2025. https://doi.org/10.1351/goldbook.13993 (accessed 9 November 2026).
4. A. Bogaerts, G. Centi, Plasma Technology for CO2 Conversion: A Personal Perspective on Prospects and Gaps, Frontiers in Energy Research 8 (2020) 111. https://doi.org/10.3389/fenrg.2020.00111.
5. A. Mukhtar, S. Saqib, D. Mohotti, R. Ndeddy Aka Jr., M. Hossain, E. Agyekum-Oduro, S. Wu, Non-thermal plasma-catalytic processes for CO_2 conversion toward circular economy: fundamentals, current status, and future challenges, Environmental Science and Pollution Research 32 (2025) 27314−27334. https://doi.org/10.1007/s11356-024-34751-3.
6. P. Mierczyński, A. Mierczynska-Vasilev, M.I. Szynkowska-Jóźwik, K. Ostrikov, K. Vasilev, Plasma-assisted catalysis for CH_4 and CO_2 conversion, Catalysis Communications 180 (2023) 106709. https://doi.org/10.1016/j.catcom.2023.106709.
7. X. Chen, H.-H. Kim, T. Nozaki, Plasma catalytic technology for CH_4 and CO_2 conversion: A review highlighting fluidized-bed plasma reactor, Plasma Processes and Polymers 21 (2024) 2200207. https://doi.org/10.1002/ppap.202200207.
8. E.C. Neyts, K. Ostrikov, M.K. Sunkara, A. Bogaerts, Plasma catalysis: synergistic effects at the nanoscale, Chemical Reviews 115 (2015) 13408−13446. https://doi.org/10.1021/acs.chemrev.5b00362.
9. A. Bogaerts, X. Tu, J.C. Whitehead, G. Centi, L. Lefferts, O. Guaitella, et al., The 2020 plasma catalysis roadmap, Journal of Physics D: Applied Physics 53 (2020) 443001. https://doi.org/10.1088/1361-6463/ab9048.
10. J. Huang, J. Wang, H. Guo, Plasma-Catalytic CO_2-to-Energy Conversion: Fundamentals, Applications, Challenges, and Perspectives, Catalysts 16 (2026) 514. https://doi.org/10.3390/catal16060514.
11. Q. Huang, Z. Liang, F. Qi, N. Zhang, J. Yang, J. Liu, C. Tian, C. Fu, X. Tang, D. Wu, J. Wang, X. Wang, W. Chen, Carbon dioxide conversion synergistically activated by dielectric barrier discharge plasma and the $CsPbBr_3$@TiO_2 photocatalyst, Journal of Physical Chemistry Letters 13 (2022) 2418−2427. https://doi.org/10.1021/acs.jpclett.2c00253.

12. P.J. Bruggeman, M.J. Kushner, B.R. Locke, J.G.E. Gardeniers, W.G. Graham, D.B. Graves, et al., Plasma−liquid interactions: a review and roadmap, Plasma Sources Science and Technology 25 (2016) 053002. https://doi.org/10.1088/0963-0252/25/5/053002.
13. M.Y. Ong, S. Nomanbhay, F. Kusumo, P.L. Show, Application of microwave plasma technology to convert carbon dioxide (CO_2) into high value products: A review, Journal of Cleaner Production 336 (2022) 130447. https://doi.org/10.1016/j.jclepro.2022.130447.
14. T. Ihara, M. Kiboku, Y. Iriyama, Plasma reduction of CO_2 with H_2O for the formation of organic compounds, Bulletin of the Chemical Society of Japan 67 (1994) 312−314. https://doi.org/10.1246/bcsj.67.312.
15. T. Ihara, T. Ouro, T. Ochiai, M. Kiboku, Y. Iriyama, Formation of methanol by microwave-plasma reduction of CO_2 with H_2O, Bulletin of the Chemical Society of Japan 69 (1996) 241−244. https://doi.org/10.1246/bcsj.69.241.
16. G. Chen, T. Silva, V. Georgieva, T. Godfroid, N. Britun, R. Snyders, M.-P. Delplancke-Ogletree, Simultaneous dissociation of CO_2 and H_2O to syngas in a surface-wave microwave discharge, International Journal of Hydrogen Energy 40 (2015) 3789−3796. https://doi.org/10.1016/j.ijhydene.2015.01.084.
17. R. Snoeckx, A. Ozkan, F. Reniers, A. Bogaerts, The quest for value-added products from carbon dioxide and water in a dielectric barrier discharge: a chemical kinetics study, ChemSusChem 10 (2017) 409−424. https://doi.org/10.1002/cssc.201601234.
18. G. Chen, T. Godfroid, N. Britun, V. Georgieva, M.-P. Delplancke-Ogletree, R. Snyders, Plasma-catalytic conversion of CO_2 and CO_2/H_2O in a surface-wave sustained microwave discharge, Applied Catalysis B: Environmental 214 (2017) 114−125. https://doi.org/10.1016/j.apcatb.2017.05.032.
19. X. Ma, S. Li, M. Ronda-Lloret, R. Chaudhary, L. Lin, G. van Rooij, F. Gallucci, G. Rothenberg, N.R. Shiju, V. Hessel, Plasma assisted catalytic conversion of CO_2 and H_2O over Ni/Al_2O_3 in a DBD reactor, Plasma Chemistry and Plasma Processing 39 (2019) 109−124. https://doi.org/10.1007/s11090-018-9931-1.
20. X. Yao, Y. Zhang, Z. Wei, M. Chen, W. Shangguan, Plasma-catalytic conversion of CO_2 and H_2O into H_2, CO, and traces of CH_4 over NiO/cordierite catalysts, Industrial & Engineering Chemistry Research 59 (2020) 19133−19144. https://doi.org/10.1021/acs.iecr.0c01764.
21. P. Chawdhury, S. Chansai, M. Conway, J. Parker, M. Lindley, C.E. Stere, M. Sankar, S.J. Haigh, B. Dennis-Smither, S.V. Filip, S. Poulston, P. Hinde, C. Hawkins, C. Hardacre, Enhancing the reaction of CO_2 and H_2O using catalysts within a nonthermal plasma, ACS Catalysis 15 (2025) 7053−7065. https://doi.org/10.1021/acscatal.5c00747.
22. D. Ray, P. Ye, J.C. Yu, C. Song, Recent progress in plasma-catalytic conversion of CO_2 to chemicals and fuels, Catalysis Today 423 (2023) 113973. https://doi.org/10.1016/j.cattod.2022.12.004.

23. P. Rumbach, D.M. Bartels, R.M. Sankaran, D.B. Go, The solvation of electrons by an atmospheric-pressure plasma, Nature Communications 6 (2015) 7248. https://doi.org/10.1038/ncomms8248. Corrigendum: Nature Communications 7 (2016) 11911. https://doi.org/10.1038/ncomms11911.
24. S. Yang, B. Zhao, I.A. Aravind, Y. Wang, B. Zhang, S. Weng, Z. Cai, R. Li, A. Zarei Baygi, A. Smith, M.A. Gundersen, S.B. Cronin, CO_2 reduction to higher hydrocarbons by plasma discharge in carbonated water, ACS Energy Letters 6 (2021) 3924−3930. https://doi.org/10.1021/acsenergylett.1c01666.
25. P. Rumbach, R. Xu, D.B. Go, Electrochemical production of oxalate and formate from CO_2 by solvated electrons produced using an atmospheric-pressure plasma, Journal of The Electrochemical Society 163 (2016) F1157−F1161. https://doi.org/10.1149/2.0521610jes.
26. T. Zhang, J. Knezevic, M. Zhu, J. Hong, R. Zhou, Q. Song, L. Ding, J. Sun, D. Liu, K.K. Ostrikov, R. Zhou, P.J. Cullen, Catalyst-free carbon dioxide conversion in water facilitated by pulse discharges, Journal of the American Chemical Society 145 (2023) 28233−28239. https://doi.org/10.1021/jacs.3c11102.
27. Q. Chen, J. Li, Q. Chen, K. Ostrikov, Recent advances towards aqueous hydrogen peroxide formation in a direct current plasma−liquid system, High Voltage 7 (2022) 405−419. https://doi.org/10.1049/hve2.12189.
28. S. Nomura, H. Toyota, Sonoplasma generated by a combination of ultrasonic waves and microwave irradiation, Applied Physics Letters 83 (2003) 4503−4505. https://doi.org/10.1063/1.1631062.
29. S. Nomura, H. Toyota, S. Mukasa, Y. Takahashi, T. Maehara, A. Kawashima, H. Yamashita, Discharge characteristics of microwave and high-frequency in-liquid plasma in water, Applied Physics Express 1 (2008) 046002. https://doi.org/10.1143/APEX.1.046002.
30. S. Mukasa, T. Maehara, S. Nomura, H. Toyota, A. Kawashima, Y. Hattori, Y. Hashimoto, H. Yamashita, Growth of bubbles containing plasma in water by high-frequency irradiation, International Journal of Heat and Mass Transfer 53 (2010) 3067−3074. https://doi.org/10.1016/j.ijheatmasstransfer.2010.03.021.
31. R. Shiba, S. Nomura, A. Kakubo, K. Baba, R. Shimizu, J. Nakajima, T. Henmi, Formation of selected organic compounds from aqueous sodium carbonate solution via hetero-coupling of carbon and hydrogen by in-liquid plasma, Journal of CO2 Utilization 99 (2025) 103159. https://doi.org/10.1016/j.jcou.2025.103159.
32. R. Shiba, S. Nomura, J. Nakajima, R. Shimizu, A. Imai, T. Henmi, Synthesis of liquid fuel using water and carbon dioxide as feedstocks by in-liquid plasma, Journal of the Japan Institute of Energy 105 (2026) 185−189. https://doi.org/10.3775/jie.105.185.
33. R. Shiraishi, S. Nomura, S. Mukasa, R. Nakano, R. Kamatoko, Effect of catalytic electrode and plate for methanol decomposition by in-liquid plasma, International

Journal of Hydrogen Energy 43 (2018) 4305−4310. https://doi.org/10.1016/j.ijhydene.2018.01.060.

34. B. Eliasson, U. Kogelschatz, B. Xue, L.-M. Zhou, Hydrogenation of carbon dioxide to methanol with a discharge-activated catalyst, Industrial & Engineering Chemistry Research 37 (1998) 3350−3357. https://doi.org/10.1021/ie9709401.
35. L. Wang, Y. Yi, H. Guo, X. Tu, Atmospheric pressure and room temperature synthesis of methanol through plasma-catalytic hydrogenation of CO_2, ACS Catalysis 8 (2018) 90−100. https://doi.org/10.1021/acscatal.7b02733.
36. Y. Wang, J. Yang, Y. Sun, D. Ye, B. Shan, S.C.E. Tsang, X. Tu, Engineering Ni-Co bimetallic interfaces for ambient plasma-catalytic CO_2 hydrogenation to methanol, Chem 10 (2024) 2590−2606. https://doi.org/10.1016/j.chempr.2024.06.022.
37. D. Li, V. Rohani, A.P. Ramaswamy, M. Sennour, F. Georgi, P. Dupont, L. Fulcheri, Orientating the plasma-catalytic conversion of CO_2 and CH_4 toward liquid products by using a composite catalytic bed, Applied Catalysis A: General 650 (2023) 119015. https://doi.org/10.1016/j.apcata.2022.119015.
38. L. Wang, Y. Yi, C. Wu, H. Guo, X. Tu, One-step reforming of CO_2 and CH_4 into high-value liquid chemicals and fuels at room temperature by plasma-driven catalysis, Angewandte Chemie International Edition 56 (2017) 13679−13683. https://doi.org/10.1002/anie.201707131.
39. S. Meng, Z. Cui, Q. Chen, H. Zhang, S. Li, E.C. Neyts, E. Vlasov, K. Jenkinson, S. Bals, D. Yang, M. Liu, Y. Liu, A. Bogaerts, A.-H. Lu, Y. Yi, Water-promoted C−C coupling reaction in plasma-catalytic CO_2 hydrogenation for ethanol production, ACS Catalysis 15 (2025) 3236−3246. https://doi.org/10.1021/acscatal.4c06543.
40. S. Xu, M.E. Potter, R. Simancas, L. Costley-Wood, B. Qiu, X. Liu, et al., Unveiling active sites and the cooperative role of non-thermal plasma and copper−zinc catalysts in the hydrogenation of CO_2 to methanol, Nature Catalysis 9 (2026) 134−147. https://doi.org/10.1038/s41929-025-01477-5.
41. V. Longo, G. Centi, S. Perathoner, C. Genovese, CO_2 utilisation with plasma technologies, Current Opinion in Green and Sustainable Chemistry 46 (2024) 100893. https://doi.org/10.1016/j.cogsc.2024.100893.
42. Y. Wang, M.D. LeVan, Adsorption equilibrium of carbon dioxide and water vapor on zeolites 5A and 13X and silica gel: pure components, Journal of Chemical & Engineering Data 54 (2009) 2839−2844. https://doi.org/10.1021/je800900a.
43. R. Vertongen, G. De Felice, H. van den Bogaard, F. Gallucci, A. Bogaerts, S. Li, Sorption-enhanced dry reforming of methane in a DBD plasma reactor for single-stage carbon capture and utilization, ACS Sustainable Chemistry & Engineering 12 (2024) 10841−10853. https://doi.org/10.1021/acssuschemeng.4c02502.

44. P. Kaliyappan, A. Paulus, J. D'Haen, P. Samyn, Y. Uytdenhouwen, N. Hafezkhiabani, A. Bogaerts, V. Meynen, K. Elen, A. Hardy, M.K. Van Bael, Probing the impact of material properties of core-shell SiO_2@TiO_2 spheres on the plasma-catalytic CO_2 dissociation using a packed bed DBD plasma reactor, Journal of CO2 Utilization 46 (2021) 101468. https://doi.org/10.1016/j.jcou.2021.101468.
45. L.A. Currie, Nomenclature in evaluation of analytical methods including detection and quantification capabilities (IUPAC Recommendations 1995), Pure and Applied Chemistry 67 (1995) 1699−1723. https://doi.org/10.1351/pac199567101699.
46. M. Thompson, S.L.R. Ellison, R. Wood, Harmonized guidelines for single-laboratory validation of methods of analysis (IUPAC Technical Report), Pure and Applied Chemistry 74 (2002) 835−855. https://doi.org/10.1351/pac200274050835.
47. M. Hori, Radical-controlled plasma processes, Reviews of Modern Plasma Physics 6 (2022) 36. https://doi.org/10.1007/s41614-022-00084-2.
48. S. Schüttler, L. Jolmes, E. Jeß, K. Tschulik, J. Golda, Validation of in situ diagnostics for the detection of OH and H_2O_2 in liquids treated by a humid atmospheric pressure plasma jet, Plasma Processes and Polymers 21 (2024) 2300079. https://doi.org/10.1002/ppap.202300079.
49. A.H. Babikir, M.G.M. Ekanayake, O. Oloye, J.D. Riches, K.K. Ostrikov, A.P. O'Mullane, Plasma-Assisted CO_2 Reduction into Nanocarbon in Water Using Sonochemically Dispersed Liquid Gallium, Advanced Functional Materials 34 (2024) 2307846. https://doi.org/10.1002/adfm.202307846.
50. K. Stapelmann, S. Gershman, V. Miller, Plasma−liquid interactions in the presence of organic matter—A perspective, Journal of Applied Physics 135 (2024) 160901. https://doi.org/10.1063/5.0203125.
51. International Union of Pure and Applied Chemistry, Activation energy, in: Compendium of Chemical Terminology, 5th ed., 2025. https://doi.org/10.1351/goldbook.A00102 (accessed 9 November 2026).
52. Y. Yin, T. Yang, Z. Li, E. Devid, D. Auerbach, A.W. Kleyn, CO_2 conversion by plasma: how to get efficient CO_2 conversion and high energy efficiency, Physical Chemistry Chemical Physics 23 (2021) 7974−7987. https://doi.org/10.1039/D0CP05275B.